Intratumoral Thermal Reading During Photo-Thermal Therapy by Multifunctional Fluorescent Nanoparticles

*Elisa Carrasco, Blanca del Rosal, Francisco Sanz-Rodríguez, Ángeles Juarranz de la Fuente, Patricia Haro Gonzalez, Ueslen Rocha, Kagola Upendra Kumar, Carlos Jacinto, José García Solé, and Daniel Jaque**

The tremendous development of nanotechnology is bringing us closer to the dream of clinical application of nanoparticles in photothermal therapies of tumors. This requires the use of specific nanoparticles that must be highly biocompatible, efficient light-to-heat converters and fluorescent markers. Temperature reading by the heating nanoparticles during therapy appears of paramount importance to keep at a minimum the collateral damage that could arise from undesirable excessive heating. In this work, this thermally controlled therapy is possible by using Nd^{3+} ion-doped LaF_3 nanocrystals. Because of the particular optical features of Nd^{3+} ions at high doping concentrations, these nanoparticles are capable of in vivo photothermal heating, fluorescent tumor localization and intratumoral thermal sensing. The successful photothermal therapy experiments here presented highlight the importance of controlling therapy parameters based on intratumoral temperature measurements instead of on the traditionally used skin temperature measurements. In fact, significant differences between intratumoral and skin temperatures do exist and could lead to the appearance of excessive collateral damage. These results open a new avenue for the real application of nanoparticle-based photothermal therapy at clinical level.

1. Introduction

The battle against cancer is continuously bringing about new challenges and difficulties that can only be overcome if faced from a multidisciplinary point of view, taking advantage of the synergies between very different but complementary research areas such as biology, medicine, physics, chemistry and mathematics. Among the different ongoing multidisciplinary research lines focusing on cancer and many other diseases, great attention is being paid to the development of new materials and techniques that would improve detection and therapy. Nanotechnology is playing a central role in the development of such materials and techniques.[1] In particular, during the last few years, the refinement of nanofabrication processes has led to the appearance of a large variety of nanosized materials having pre-tailored properties with potential application as biocompatible markers, drug deliverers and therapeutic agents. Among them, Luminescent Nanoparticles (hereafter L-NPs) have played a pivotal role.[2] Initially, L-NPs attracted much attention as fluorescent nanoprobes for both in vivo and in vitro imaging experiments.[3,4] This was based on the fact that small L-NPs can flow through the bloodstream, thus being distributed along the organism after intravenous injection.[5] In addition, their reduced size allows for an efficient cell

Dr. E. Carrasco
Instituto de Investigaciones Biomédicas "Alberto Sols"
CSIC-UAM
Madrid 28029, Spain
B. del Rosal, Dr. F. Sanz-Rodríguez, Dr. P. H. Gonzalez, Prof. J. G. Solé, Dr. D. Jaque
Fluorescence Imaging Group
Departamento de Física de Materiales
Facultad de Ciencias. Campus de Cantoblanco
Universidad Autónoma de Madrid
Madrid, 28049, Spain
E-mail: daniel.jaque@uam.es
Dr. F. Sanz-Rodríguez, Prof. Á. J. de la Fuente
Departamento de Biología
Facultad de Ciencias. Campus de Cantoblanco
Universidad Autónoma de Madrid.
Madrid 28049, Spain
Dr. U. Rocha, Dr. K. U. Kumar, Prof. C. Jacinto
Grupo de Fotônica e Fluidos Complexos
Instituto de Física
Universidade Federal de Alagoas
57072–970, Maceió, Alagoas, Brazil
Dr. E. Carrasco, Dr. F. Sanz-Rodríguez, Prof. Á. J. de la Fuente, Dr. D. Jaque
Instituto Ramón y Cajal de Investigación Sanitaria
Hospital Universitario Ramón y Cajal
Madrid, 28034, Spain

DOI: 10.1002/adfm.201403653

internalization that could, indeed, be boosted by an appropriate surface functionalization.[4,6] Despite the good results obtained using L-NPs as optical probes for imaging of both cancer cells and tissues, it was noticed that fluorescence probing was only one of the numerous functions that L-NPs can offer. As an example, their ability for generating specific toxic radiations activating intracellular toxic chemical reactions (such as those releasing intracellular singlet oxygen) has already been used to develop highly specific photo-activated therapies.[7] L-NPs have also been used as therapeutic carriers enabling controlled drug delivery through adequate optical excitation.[8] In general, for all these applications, L-NPs with high luminescence quantum yields (QYs) were desired, in order to ensure high excitation (pump)-to-luminescence conversion efficiencies.[9] Large QYs also allow for the use of low excitation intensities during in vivo fluorescent imaging, thus reducing possible radiation-induced collateral effects to a minimum. As a consequence, L-NPs with low QYs were systematically discarded for biological applications. From our novel point of view, this was, indeed, a mistake. When a given L-NP has a low QY, a great fraction of the excitation radiation absorbed by the NP is transformed into heat, so that the L-NP behaves as a poor luminescent probe but as a good heating nanoparticle (H-NP).[10] This is, for example, the case of gold nanoparticles (GNPs) and Carbon Nanotubes (CNTs) that have been extensively used as photothermal agents for both in vitro and in vivo experiments.[11,12] The continuous breaking into scene of efficient H-NPs has given new impetus to photothermal treatments (PTTs) that, despite having been discovered decades ago, had been weakly used for the treatment of cancer. PTTs of tumors are based on driving cancer cells above their physiological temperature (37 ºC) for a defined period of time by using an external laser beam as excitation stimulus. When the temperature of a tumor is raised above 37 °C several processes can be activated, depending on the magnitude and duration of the heating procedure.[13] Revising the literature concerning the use of H-NPs for tumor treatments in animal models (generally in mice) leads to the conclusion that efficient tumor destruction (in a day time scale) usually requires tumor heating up to 50–55 °C during, typically, 5–10 min.[14,15] The fact that many authors have already reported on successful laser-induced tumor treatment by using H-NPs has led public opinion to seriously consider nanoparticle-based PTTs as a realistic alternative therapy against cancer.

Nevertheless, before moving into pre-clinical stages with the maximum guarantee of success and in a completely safe manner, there are several concerns to be solved. The main concerns are related to the possible toxicological drawbacks of H-NPs and the undesirable collateral effects potentially caused by the thermal therapy itself. Concerning the latter aspect, it is clear that the success of the therapy, while minimizing its collateral effects (damage), requires of an accurate real time monitoring of the tumor temperature during the in vivo treatment. This would be the only way to avoid excessive heating not only of the tumor but also of the surrounding tissue. In many in vivo photothermal treatments such a thermal control has been attempted by using "conventional" infrared thermometry, based on an appropriate analysis of the blackbody radiation emitted by the treated tumor.[16,17] This is quite a versatile technique that has provided suitable results in the past. Nevertheless, this strategy has a remarkable limitation that went unnoticed for many researchers; it does only provide information about the surface temperature (just at the skin level). This is a crucial point, since the actual temperature of subcutaneous tumors could significantly differ from that of the skin surface.[18] The existence of this difference resides on the heat diffusion process from the sub-tissue heating source (H-NPs) to the skin surface.[19] In addition, temperature sensing and imaging by infrared thermometry is not exempt of experimental uncertainties. For example, the magnitude of the surface temperature measured by infrared thermometry could be strongly dependent on the relative orientation (angle) between the IR camera and the measured surface, so that changes in the relative position of the small animal during in vivo procedures could affect the measured temperature.[20] Therefore, efficient and selective PTTs still have to overcome the challenge of real time and accurate intratumoral temperature sensing.

Sub-tissue (intratumoral) thermal sensing is far from being a simple task. Obviously, for the purpose of tumor treatment, this thermal sensing has to be achieved without involving any physical contact. Luminescence nanothermometry is a very attractive option in which L-NPs act as thermal sensors based on an appropriate analysis of their fluorescent properties, which should be affected by temperature variation within the physiological range (30–60 °C).[21,22] Luminescent Nanothermometers (L-NThs) have already been used to provide real time thermal reading during PTTs in both culture cells and living organisms.[23,24] In both cases, PTTs were based on the combination of independent H-NP and L-NThs into a single platform or coexisting in the same colloidal solution.[25] Furthermore, although this approach provided very good results, its application for real time sub-tissue tumor treatment is restricted by the fact that the used L-NThs operate in the visible spectral range and, thus, their optical penetration depth into tissues is very limited.[26] Overcoming this limitation implies the use of L-NThs operating in the infrared biological spectral windows (covering from 700 up to 1400 nm). Several fluorescent NPs (such as Carbon Nanotubes, Rare earth doped Nanoparticles and infrared emitting Quantum Dots) have already been reported as efficient infrared nanoprobes capable of deep tissue bioimaging but not for thermal sensing purposes.[27] In addition to the penetration issue, the need of using two different types of nanostructures (one for heating and the other for temperature reading) is undesirable, since their different properties could lead to different biodistribution pathways, so that their spatial overlap is not guaranteed. This could be overcome by combining in a single structure two types of NPs (nanothermometer + nanoheater) mechanically linked. Such multifunctional structures have already been fabricated, providing good results although with limited application for in vivo therapies as, again, they operate in the visible spectral range.[28] In addition, the mechanical stability of the link between the two NPs could also be a limiting factor.

In order to avoid all these limitations, a single infrared-emitting NP capable of simultaneous heating and infrared luminescence thermometry would be required. In this context, Neodymium ions (Nd^{3+}) doped NPs have recently emerged as breaking candidates with outstanding properties, such as efficient infrared emission in the biological windows, relevant

thermal sensitivity of their fluorescence bands and, what provides heating capabilities, a variable light-to-heat conversion efficiency.[29] Despite this unique combination, the potential use of Nd^{3+} doped NPs as intratumoral thermal sensors and photothermal agents for in vivo treatment remained as an unachievable dream. In this work this dream has turned into reality as we demonstrate real in vivo PTTs with real time intratumoral thermal reading by using heavily Nd^{3+} doped NPs acting simultaneously as nanoheaters and luminescent nanothermometers.

2. Results and Discussion

As it has been previously mentioned, the most interesting and breaking benefit of using Nd^{3+}-doped NPs is that they offer the possibility of tailoring the balance between light and heat generation through an appropriate choice of the Nd^{3+} concentration inside the NP.[29] This possibility is schematically illustrated in **Figure 1**. When the concentration of Nd^{3+} ions inside the LaF_3 NP is low (what we call in this work "diluted" NPs) then the interaction between ions is kept at a minimum. In this case, the absorbed radiation is re-emitted in the form of luminescence without any appreciable heat generation (light is converted into light).[10] This fact is demonstrated in the top row of Figure 1a, which includes an optical image of an aqueous solution of diluted Nd^{3+} doped LaF_3 NPs (doping level was 0.2 at%) as well as the infrared (emission wavelengths > 850 nm) fluorescence and thermal images under optical excitation with a 1 W/cm^2 808 nm laser beam. Note that the actual Neodymium content inside the LaF_3 NPs has been experimentally determined by performing EDX experiments that confirm a Neodymium incorporation efficiency close to 92% during the synthesis procedure (see Figure S1 in the Supporting Information). As can be observed, when the Nd^{3+} content is low, optical excitation leads to luminescence generation while no heating is produced. In this case, Nd:LaF_3 NPs behave as high brightness luminescent probes. On the other hand, when the concentration of Nd^{3+} ions inside the NP is increased, leading to "dense" Nd^{3+} doped NPs, heat is generated as a consequence of both the increase in the absorbed pump power and the reduction in the fluorescence quantum yield.[10] The simultaneous generation of luminescence and heat is also schematically illustrated and experimentally demonstrated in Figure 1b. As can be observed, when a solution of "dense" Nd:LaF_3 NPs (5.6 at% doping level) is optically excited with a 808 nm laser beam it simultaneously generates luminescence and heat. Thus, Figure 1a,b provides evidence that increasing the Nd^{3+} doping level gives Nd:LaF_3 NPs heating capabilities while still being luminescent, in such a way that they behave as multifunctional luminescent nanoparticles. From Figure 1a,b it is clear that diluted samples generate more luminescence but less heat. In order to make this effect even clearer, we have performed a systematic study by recording both the fluorescence and thermal images of up to 8 samples with different Nd^{3+} concentrations. From the obtained images, all included in the Supporting Information (see Figure S2), we determined how both the luminescence intensity and pump-induced heating vary with the Nd^{3+} concentration (Figure 1c). The laser-to-heat conversion efficiency increases monotonously with the Neodymium content whereas the

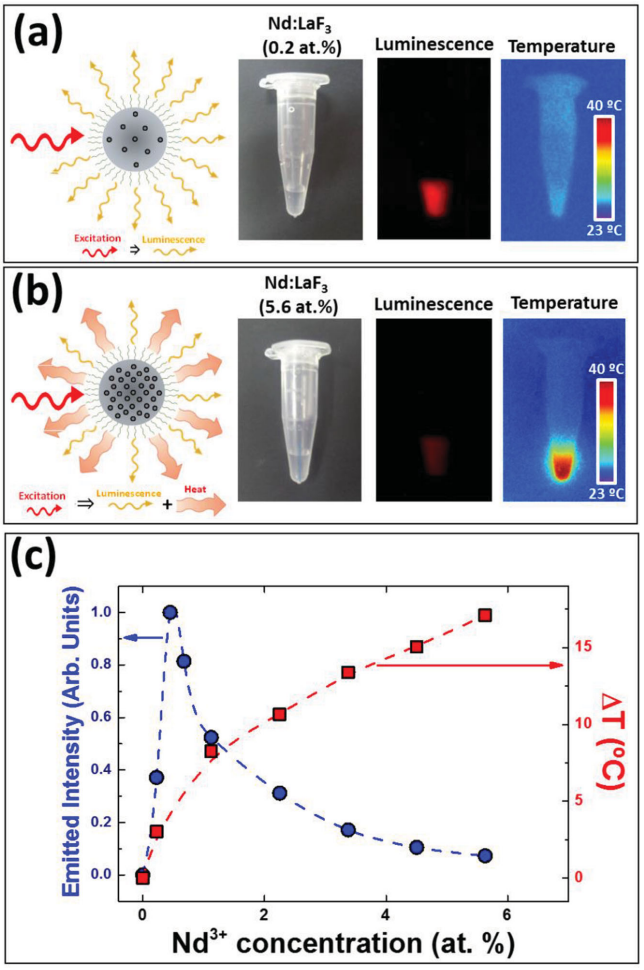

Figure 1. Schematic representation of the light-matter interaction processes activated by a Rare Earth doped nanoparticle when optically excited. a,b) The case of "diluted" and "dense" nanoparticles (corresponding to Neodymium concentrations of 0.2 and 5.6 at%, respectively). For each case, we have included the optical image of the tube containing an aqueous solution of Nd:LaF_3 NPs together with the fluorescence and thermal image of the same solution under 808 nm optical excitation. In both cases the NP concentration inside the solution was set to 1% in mass. Note that appreciable light-to-heat conversion is only produced in heavily doped NPs. c) The variations of integrated emitted intensity and of the 808 nm laser induced heating as a function of the Neodymium content inside the LaF_3 NPs. Dots are experimental data and dashed lines are guides for the eyes.

luminescence intensity follows a more complicated trend. At low Nd^{3+} concentrations (below 0.5 at%) the emission intensity increases with Nd^{3+} content. For such low concentrations, the luminescence quantum yield (η_{lum}) remains constant but the absorbed pump power increases with Nd^{3+} concentration due to the increment in the absorption coefficient, as is evidenced in the absorption spectra included in **Figure 2**a. Furthermore, systematic absorption studies have revealed that the absorption coefficient of Nd:LaF_3 NPs is proportional to the Nd^{3+}, as it is shown in the Supporting Information (Figure S1). On the other hand, at concentrations above 0.5 at%, the luminescence brightness decreases with the Neodymium content as a result of concentration-induced quenching (concentration-induced QY

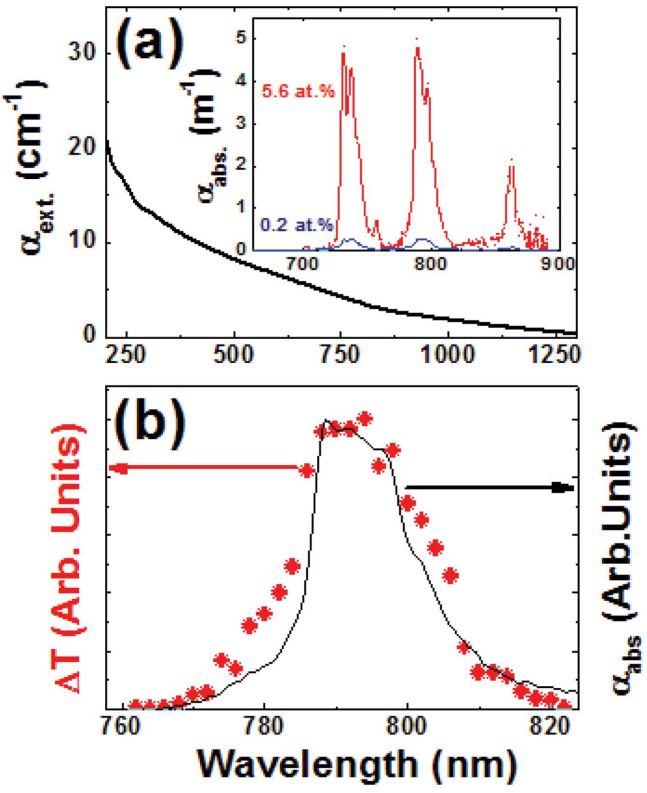

Figure 2. a) Room temperature extinction coefficient in the 200–1400 nm spectral range as obtained for colloidal solutions of Nd:LaF_3 nanoparticles. The nanoparticle concentration was set to 10 mg/mL (1% in mass). Inset shows the absorption coefficient in the 650–900 nm spectral range as obtained by subtracting the scattering background. Red and blue lines correspond to the absorption spectra obtained for the 5.6 and 0.2 at% Neodymium doped samples, respectively. b) Detail of the room temperature absorption spectrum of Nd:LaF_3 nanoparticles (5.6 at% Neodymium doped) in the 750–830 nm range (solid line). Dots show the wavelength dependence of the laser-induced temperature increment produced in Nd:LaF_3 nanoparticles by using a tunable Ti:Sapphire laser.

reduction). Therefore, the luminescence intensity vs Nd^{3+} concentration curve of Figure 1c can be understood by the interplay between both concentration-induced absorption increment and concentration-induced luminescence quenching, as has already been predicted for Nd:LaF_3 NPs and experimentally observed in a great variety of Neodymium doped luminescent systems.[10,30] At this point, it should be noted that the modification of the Nd^{3+} content leads to a drastic change in the luminescence intensity but the luminescence shape is not severely affected, as can be observed in the luminescence spectra included in the Supporting Information (Figure S3). The concentration dependence of the pump-induced heating efficiency (see Figure 1c) can be understood, in a first order approximation, taking into account that the pump-induced heating (ΔT) is proportional to the amount of pump power that is absorbed by the NPs multiplied by the fractional thermal loading (ϕ_{heat}) of the NPs in such a way that: $\Delta T \propto P_{abs}\phi_{heat}$. The fractional thermal loading is the fraction of absorbed pump energy that is transformed into heat. This depends on the luminescence quantum yield, the pump wavelength (λ_{pump} = 808 nm in our experiments) and on the average luminescence wavelength of Nd:LaF_3 NPs ($\lambda_{lum} \approx 1000$ nm) so that it is given by $\phi_{heat} = \left(1 - \eta_{lum}\frac{\lambda_{pump}}{\lambda_{lum}}\right)$. For the case of heat generation, both terms involved (P_{abs} and ϕ_{heat}) increase with the Nd^{3+} content and, therefore, the pump-to-heat conversion efficiency is expected to increase with the Nd^{3+} content (as has been experimentally observed in Figure 1c). The dominant mechanism leading to the higher pump-to-heat conversion efficiency at high Nd^{3+} contents can be tentatively identified by a simple calculation. The experimentally determined luminescence quantum yields are 0.8 and 0.2, for the 0.2 and 5.6 at% doped samples, respectively ($\eta_{lum}(0.2\,at\%) = 0.8$ and $\eta_{lum}(5.6\,at\%) = 0.2$). As a consequence, the ratio between the corresponding fractional thermal loadings is $\frac{\phi_{heat}(5.6\,at\%)}{\phi_{heat}(0.2\,at\%)} = \frac{0.84}{0.34} \approx 2$. From Figure 1c, we can see that the ratio between the measured temperature increments in the 0.2 and 5.6 at% samples is close to 6 ($\frac{\Delta T(5.6\,at\%)}{\Delta T(0.2\,at\%)} \approx 6$). Therefore, the concentration-induced increase in the fractional thermal loading (due to luminescence quenching) only accounts for one third of the experimentally observed increment in the pump-to-heat conversion efficiency. This estimation points out that the dominant contribution to the high laser-to heat conversion efficiencies observed in heavily doped samples is the increase in the absorption coefficient due to the increase in the Nd^{3+} content. At this point, we would like to note that the absorption coefficient of Nd:LaF_3 NPs does not only determine the magnitude of the pump-induced heating but also its wavelength dependence. Figure 2 shows a detail of the absorption coefficient of Nd:LaF_3 NPs (solid line) together with the wavelength dependence of the pump-induced heating as obtained by using a continuous wave Ti:Sapphire tunable laser. As can be observed, heat generation well follows the spectral dependence of the absorption coefficient revealing non-radiative de-excitation from electronic levels of Nd^{3+} ions as the only heating source.

For the particular case of Nd:LaF_3 NPs, this dual functionality (luminescence and heat generation) is accompanied by the additional capability of luminescence thermal sensing (nanothermometry).[30] The emission spectrum of dense Nd:LaF_3 NPs in the 850–930 nm infrared wavelength range is shown in **Figure 3**a. It consists of different superimposed bands, corresponding to electronic transitions between different Stark sublevels of the $^4F_{3/2}$ (excited) and $^4I_{9/2}$ (ground) electronic states of Nd^{3+} ions.[10] Interestingly, the ratio between emitted intensities at around 865 and 885 nm (spectral ranges marked in Figure 3a as IR1 and IR2, respectively) varies linearly with temperature in the biological thermal range (see Figure 3b). Consequently, the dynamical monitoring of this spectral ratio could provide intratumoral thermal sensing during photothermal therapy. Let us remember again that this luminescent thermal sensing would be accompanied by a remarkable laser-induced heat generation, in such a way that dense Nd:LaF_3 NPs behave simultaneously as luminescent probes, therapeutic heating agents and luminescent nanothermometers. This combination makes Nd:LaF_3 NPs unique candidates for the development of single platforms for dynamically controlled in vivo thermal treatments of tumors. From experimental data included in Figure 3b we have

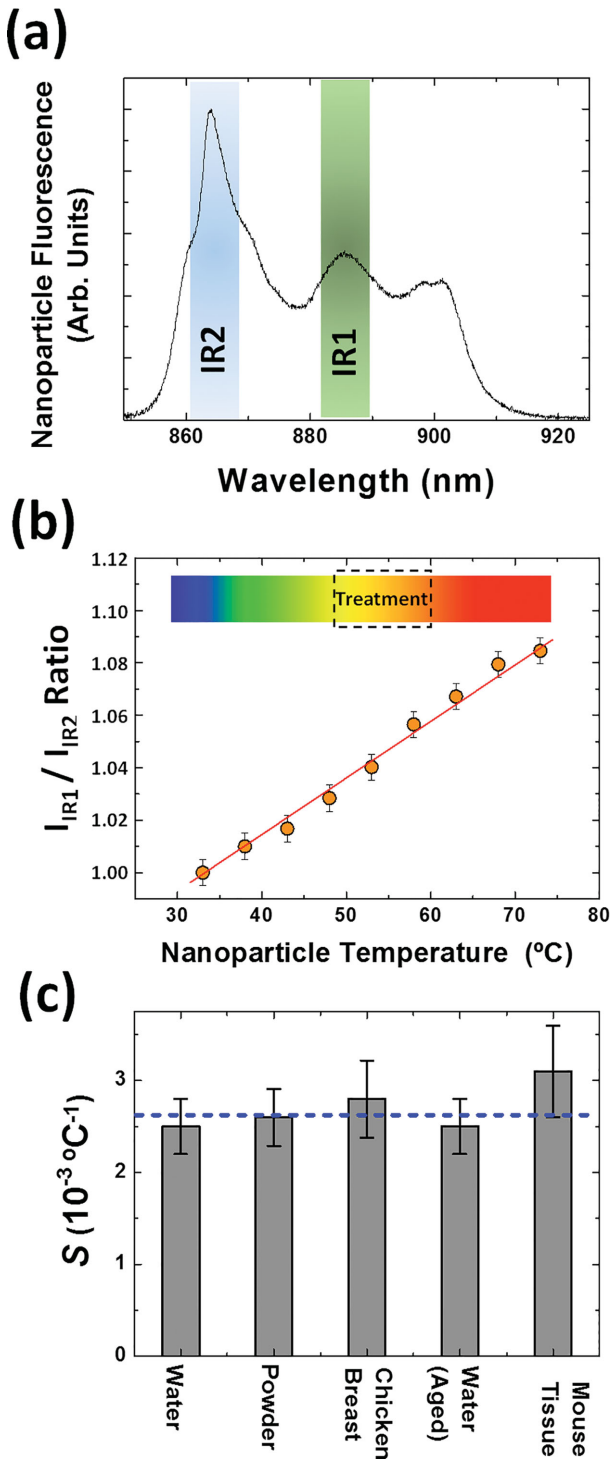

Figure 3. a) Near infrared (850–930 nm) room temperature emission spectra of heavily (5.6 at%) doped Nd:LaF_3 NPs. The two spectral ranges used for ratiometric fluorescence thermal sensing (IR1 and IR2) are schematically indicated. b) Temperature dependence of the IR1/IR2 intensity ratio. Dots are experimental data and solid line is the best linear fit. The temperature range required for efficient photo-thermal treatment of tumors is schematically indicated. c) Thermal sensitivities (*S*, as defined in the text) of Nd:LaF_3 nanoparticles as obtained in different environments. Dashed line is a guide for the eye indicating an averaged estimated value for the thermal sensitivity.

calculated the thermal sensitivity (*S*) of the Nd:LaF_3 NPs following the standard definition given by V. Kumar that applies for ratiometric luminescent temperature sensors:[31]

$$S = \frac{1}{R}\frac{dR}{dT} \quad (1)$$

where *R* is the IR1/IR2 luminescence ratio. From the experimental data we have obtained, for an aqueous solution of Nd:LaF_3 NPs, a thermal sensitivity of 2.5×10^{-3} C^{-1}. This value can now be compared to the ratiometric thermal sensitivities previously reported for other rare earth based ratiometric luminescent nanothermometers that are listed in **Table 1**. Table 1 includes the thermal sensitivities of different NPs as well as their corresponding spectral operating ranges. A critical inspection of this Table reveals that the thermal sensitivity of the Nd:LaF_3 NPs is almost one order of magnitude smaller than, for instance, those reported for the widely used Er:Yb codoped nanoparticles.[22] Nevertheless, when compared with the thermal sensitivities reported for nanoparticles working in the infrared biological window we have found that Nd:LaF_3 nanoparticles show the highest thermal sensitivity. At this point, it should also be noted that a luminescent nanothermometer that is to be used in a bio-system should have an environment-independent thermal sensitivity. Indeed, it is possible to find in the literature some examples of fluorescence nanothermometers whose sensitivity (thermal response) strongly depends on the properties of the environment surrounding the NPs. This is, for instance, the case of the Green Florescent Protein (GFP) based thermometers, which show different temperature sensitivities inside the cytoplasm and in phosphate buffer saline (PBS) due to the different viscosities of both media.[23] This is a serious drawback for *in vivo* thermal reading, as it implies that the thermal response of the nanosensors could vary with changes in the tissue properties (which do occur, for instance, during photothermal treatment of cancer tumors). In our case, this is not expected, as the thermal sensitivity of Nd:LaF_3 nanoparticles arises from population redistribution among the

Table 1. Thermal sensitivities (*S*), as defined in the text, of different rare earth doped nanoparticles that have been proven to work as ratiometric fluorescent thermal sensors. The corresponding spectral operation ranges have also been included.

System	Operating wavelength	Thermal Sensitivity (*S*)	Ref.
Nd:LaF_3	≈ 900 nm	2.6×10^{-3}	This work
Tm:Yb:Eu:$NaGdF_4$	500–650 nm	2.2×10^{-3}	[36]
Yb:Tm:Y_2O_3	450–800 nm	4.0×10^{-3}	[37]
Yb:Ho:Y_2O_3	530–750 nm	$2.7.0 \times 10^{-3}$	[37]
Yb:Ho:Zn:Y_2O_3	≈ 490 nm	10.0×10^{-3}	[38]
Ho:$CaWO_4$	≈ 470 nm	21.0×10^{-3}	[39]
Er:Yb:CaF_2	≈ 550 nm	16.0×10^{-3}	[40]
Yb:Tm:CaF_2	≈ 800 nm	2.0×10^{-3}	[40]
Nd:$NaYF_4$	≈ 800 nm	1.6×10^{-3}	[41]
Nd:YAG	≈ 940 nm	1.5×10^{-3}	Private communication from A. Benayas

electronic levels of Nd^{3+} ions. Nevertheless, in order to validate this, we have measured their thermal sensitivity in different media, including aqueous solution, powder, and biological tissue samples (chicken breast, skin and muscle tissues obtained from a sacrificed mouse). The thermal sensitivities estimated in each case, obtained from a simple linear fit of the experimental data, are displayed in Figure 3c. In this graph, we have also included the thermal sensitivity obtained from water-dispersed Nd:LaF_3 nanoparticles synthesized almost three years ago (labelled as "Water (Aged)"). From Figure 3c, it is clear that even under a drastic environment change, such as water-to-air (i.e., from aqueous solution to powder), the thermal sensitivity does not change significantly. Furthermore, when "old" (aged) samples were analyzed, the same thermal sensitivity was obtained, which indicates that the temperature sensing capability of Nd:LaF_3 NPs does not degrade with time. The obtained thermal sensitivities for Nd:LaF_3 NPs incorporated into biological tissue samples were slightly different than that of water-dispersed Nd:LaF_3 NPs. At this point, it should be noted that acquiring a calibration curve of Nd:LaF_3 NPs incorporated into tissues implies several technical problems, such as tissue drying and difficulty to obtain an homogeneous tissue temperature. All these problems lead to a greater degree of uncertainty when determining the thermal sensitivity of the sub-tissue injected Nd:LaF_3 nanoparticles. Even considering the experimental uncertainties, the sensitivities obtained inside tissues can be considered, in a first order approximation, to be the same as those obtained for Nd:LaF_3 water dispersed NPs and equal, on average, to 2.6×10^{-3} °C^{-1}. Results included in Figure 3c allow us to present Nd:LaF_3 NPs as robust, environment-independent fluorescent nanothermometers.

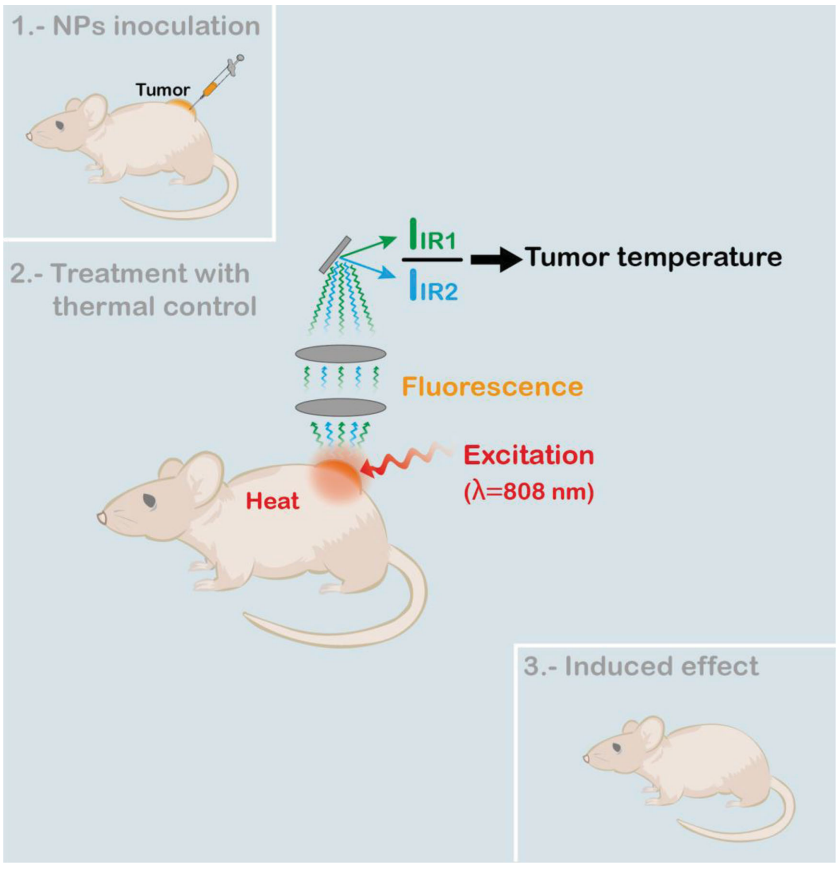

Figure 4. Schematic representation of sequential steps followed in this work for dynamically controlled photothermal treatments of tumors in mice by using "dense" Nd:LaF_3 NPs. Xenograft tumors were inoculated with a solution of NPs (Step 1). Once incorporated in the tumoral tissue, multifunctional NPs were irradiated with 808 nm laser inducing both heat and fluorescence emission (Step 2) and allowing for dynamic monitoring of intratumoral temperature. Finally, as a result of the treatment, the tumors were eliminated (Step 3).

We next evaluated the potential application of dense Nd:LaF_3 NPs for controlled photothermal therapy of human tumors using a xenograft murine animal model. For this purpose, we induced the development of subcutaneous tumors in athymic nude mice by inoculating human breast cancer cells (MDA-MB-231 line) in both flanks of each mouse. When tumor size exceeded 9 mm^3, corresponding approximately to 2 weeks after inoculation, we started photothermal therapy following the experimental methodology that is schematically represented in **Figure 4**. A solution of Nd:LaF_3 NPs dispersed in PBS at a concentration of 50 µg/ml was directly injected into the tumors. The injected volume was, in all cases, ½ of the estimated tumor volume. Once Nd:LaF_3 NPs were incorporated into the tumor we proceeded to irradiate the mouse with a 808 nm laser to complete the PTT. After laser irradiation, the time evolution of tumor volume was systematically analyzed in order to assess the efficacy of the treatment, in comparison with the corresponding control tumors. Since each mouse was inoculated in both flanks, it was possible to select pairs of tumors in the same mouse in order to compare the response of one tumor to PTT (NPs + laser irradiation) to the other tumor, which was kept as a control, either inoculated with an equivalent volume of PBS and irradiated with laser or just inoculated with NPs without laser irradiation.

Importantly, we managed to dynamically monitor the intratumoral temperature during PTT by analyzing the spectral properties of the injected Nd:LaF_3 NPs. For this purpose, we assessed the intratumoral fluorescence generated by injected Nd:LaF_3 NPs by collecting it with an optical fiber connected to a high resolution spectrometer. The ratio between IR1 and IR2 fluorescence intensities was then converted into temperature using the calibration curve included in Figure 3b. The surface temperature was simultaneously measured using an infrared thermal camera, so that it was possible to compare the intratumoral temperature with the surface (skin) one.

Figure 5a shows an optical image of a representative mouse with two tumors. The tumor on the left side was injected with a PBS solution containing Nd:LaF_3 NPs, whereas the right side one was used as a control and injected with an equivalent

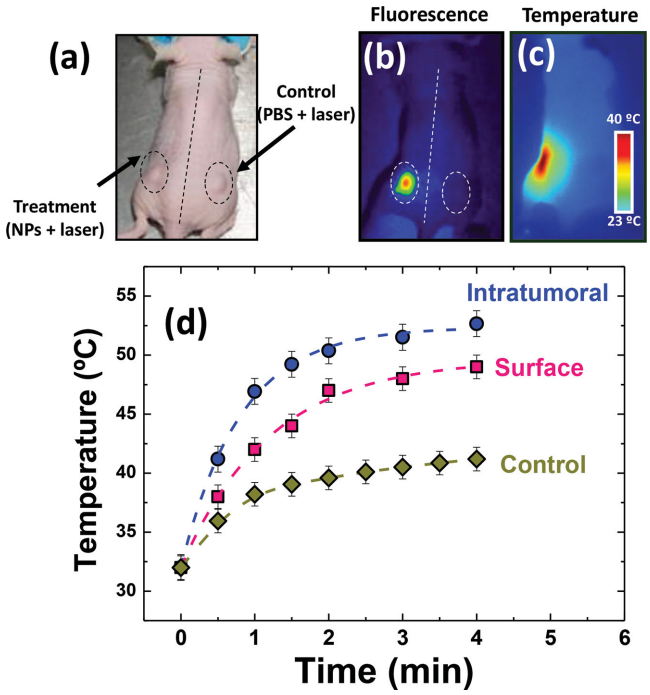

Figure 5. a) Optical image of a representative mouse with two tumors. A solution of "dense" Nd:LaF_3 NPs was injected only in the left-side tumor whereas the right-side one was used as a control. b,c) Infrared fluorescence and thermal images of the same mouse under 808 nm (4 W/cm^2) laser irradiation, respectively. The images show the fluorescent and heating signals differentially emitted by the treated tumor. d) Time evolution of the temperature at the tumor surface as obtained from the analysis of infrared thermal images. The time evolution of intratumoral temperature obtained from the analysis of sub-tissue fluorescence is also included. Symbols are experimental data and dashed lines are guides for the eyes.

volume of PBS. The presence of Nd:LaF_3 NPs in the left side tumor is evidenced from the infrared fluorescence image included in Figure 5b, in which only the left side tumor appears bright. After the injection, both tumors were subjected to 808 nm laser (4W/cm^2 intensity) irradiation. In the case of the tumor injected with Nd:LaF_3 NPs, we were able to simultaneously monitor the intratumoral and the surface temperature during laser irradiation (see infrared thermal image included in Figure 5c). Results are included in Figure 5d. As can be observed, stabilization of both inner (intratumoral) and surface temperatures was achieved about 3 min after the beginning of the treatment. Remarkably, the obtained intratumoral temperature was, on average, 20% higher than that measured at the surface. As we have previously discussed, this result was expected according to the sub-tissue location of the heating source (Nd:LaF_3 H-NPs). Heat diffusion through tissues in combination with tissue-air heat transfer causes the surface temperature to be lower than the intratumoral one.[32] Data included in Figure 5d reveal the importance of monitoring intratumoral temperature instead of assimilating it to skin temperature (as has been frequently done in the past during in vivo photothermal therapies). Figure 5d also includes the time evolution of surface temperature, corresponding to the control tumor when subjected to the same laser irradiation procedure. These data reveal that heating due to residual tissue absorption does still exist but it is less than 50% of the heating induced by Nd:LaF_3 NPs in the tumor subjected to PTT.

At this point it should be pointed out that the use of Nd:LaF_3 NPs has provided an intratumoral thermal determination overcoming the previously mentioned limitations of the widely used infrared thermometry (access to sub-tissue temperature and temperature determination not affected by geometrical conditions of the experiment). As a limitation, we should note that the use of fluorescent nanothermometers provide a local temperature measurement whereas infrared thermometry is able to provide two-dimensional thermal images (i.e., thermal images not only of the irradiated tumor but also from its surroundings), this being especially relevant when evaluating the possible presence of collateral thermal damage. Therefore, it could be recommendable the combined use of both complementary strategies.

The efficacy of the PTT was further investigated by monitoring the time evolution of the tumor size. **Figure 6** shows the results obtained in one representative mouse with two tumors, one of them subjected to PTT and the other one used as a (PBS + laser) control. Figure 6a,b shows the optical images of the same representative mouse shown in Figure 5, 15 min and 20 days after treatment, respectively. The tumors subjected to PTT (NPs+laser) sharply reduced its size during the first 5 days (see

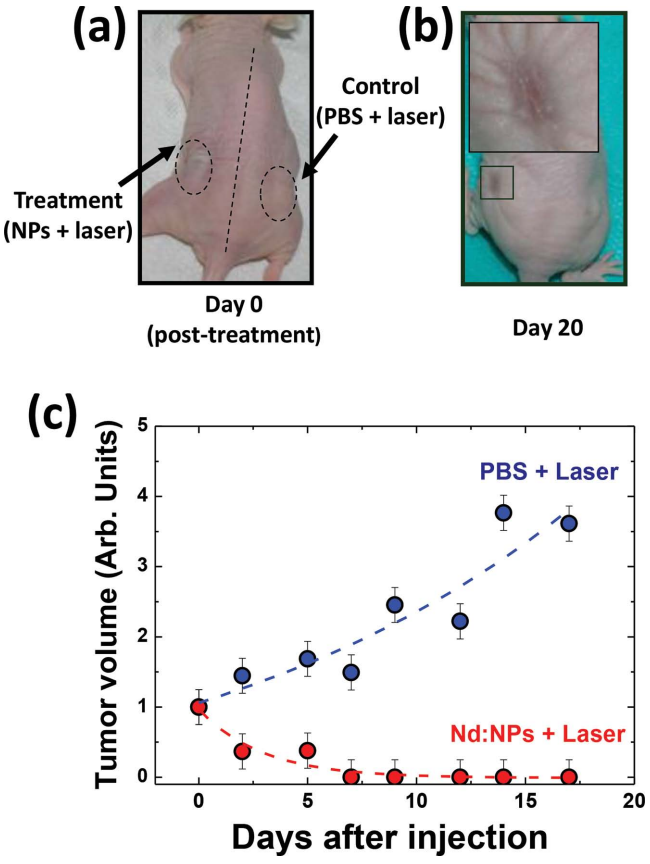

Figure 6. Optical images of the same representative mouse shown in Figure 5, a)15 min and b) 20 days after the photo thermal treatment with "dense" Nd:LaF_3 NPs and 4 W/cm^2 of 808 nm laser irradiation. The size evolution of both treated and control tumors is included in (c). Symbols are experimental data and dashed lines are guides for the eyes.

Table 2. Different nanoparticles already used for efficient in vivo photothermal treatment of cancer tumors. The parameters corresponding to the different treatment procedures are also listed for the sake of comparison.

System	Power density [W/cm^2]	Administration	Irradiation Time [min]	Dose [mg/Kg]	Intratumoral thermal reading	Ref.
Nd:LaF_3 Nanoparticles	4	Intratumoral	5	0.01	Yes	This work
Gold Nanorods	1.7–1.9	Intravenous	10	0.7	No	[15]
	0.9–1.1	Intratumoral	10			
Gold Nanoparticles	4	Intramuscular	5	2–8	No	[42]
Gold Nanorods	1.2	Intratumoral	5	2	No	[43]
Single Walled Carbon Nanotubes	1	Intratumoral	5	1	No	[44]
Single Walled Carbon Nanotubes	0.6	Intravenous	5	3.6	No	[17]
Single Walled Carbon Nanotubes	76	Intratumoral	3	0.7	No	[12]
Multi Walled Carbon Nanotubes	3	Intratumoral	0.5	5	No	[45]
Multi Walled Carbon Nanotubes	0.2	Intratumoral	10	20	No	[46]
Nano Graphene Sheets	2	Intravenous	5	20	No	[47]
Graphene Nanoparticles	0.5	Intravenous	15	2	No	[48]
Polypyrrole NPs	0.5	Intratumoral	5	10	No	[49]
PEGylated mycelle NPs	0.5	Intravenous	5	0.01	No	[50]

Figure 6c). All the animals subjected to the PTT developed an uninfected scab that gradually disappeared within a period of 15–20 days subsequent to the treatment. The only remaining sign of the preexisting tumors after 20 days was a superficial scar. In contrast, the size of the control tumors continued to increase during the 15–20 days period (see Figure 6c). In summary, a total number of 6 tumors were subjected to PTT. As a result, all the treated tumors disappeared following the evolution pattern previously described (Figure 5, 6), in contrast with the remaining control tumors. The experimental parameters used in this work for tumor treatment have been summarized in **Table 2**. For the sake of comparison, Table 2 also lists some of the different nanoparticles already used for efficient in vivo photothermal treatment of cancer tumors. The experimental parameters corresponding to the different treatment procedures are also listed for the sake of comparison.

For the assessment of possible body retention of intratumorally injected Nd:LaF_3 NPs, we collected several organs from mice euthanized 20 days after the treatment for their ex vivo fluorescence analysis under 808 nm excitation. We only found evidence of the presence of NPs at the skin scar and in the spleen, see **Figure 7**. This fact suggests that those NPs that, during or after laser irradiation, were able to leave the tumor and reach the bloodstream were finally (after 20 days) accumulated at the spleen. This would occur if the Nd:LaF_3 NPs used in this work are, for long circulating times, preferentially accumulated at the spleen. In order to verify this we investigated the biodistribution patterns obtained in CD1 mice at different times after intravenous injection of Nd:LaF_3 NPs (see Figure 7). At the shortest time analyzed (Figure 7a), NPs were mainly found at the liver and the spleen and, in a reduced proportion, at the kidneys, heart and lungs. One hour after the injection (Figure 7b), evidence of Nd:LaF_3 NPs accumulation was only found at liver and spleen, being NP accumulation larger at the liver. For longer circulation times (16 days, as shown in Figure 7c), evidence of NP retention was mainly observed at the spleen, so that there has been a time-induced NP transfer from liver to spleen. At this point, it is important to note that a similar behavior has been recently found for Nd:SrF NPs by the authors.[33] According to these observations, it is reasonable to conclude that for even longer circulation times (such as the 20 post-treatment days analyzed) NPs circulating through the bloodstream are expected to accumulate mainly at the spleen, as is pointed out by the post-treatment biodistribution pattern of Figure 7d. Furthermore,

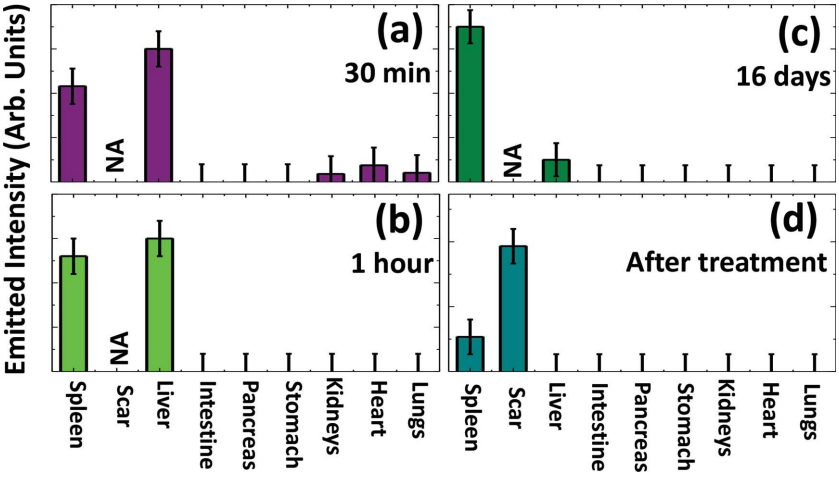

Figure 7. a–c) Biodistribution patterns obtained after intravenous injection of Nd:LaF_3 nanoparticles as obtained in CD1 mice at different times after injection (30 min, 1 h, and 16 days, respectively). d) Biodistribution pattern obtained 20 days after successful photothermal treatment of a xenograft tumor in an athymic nude mouse (Harlan).

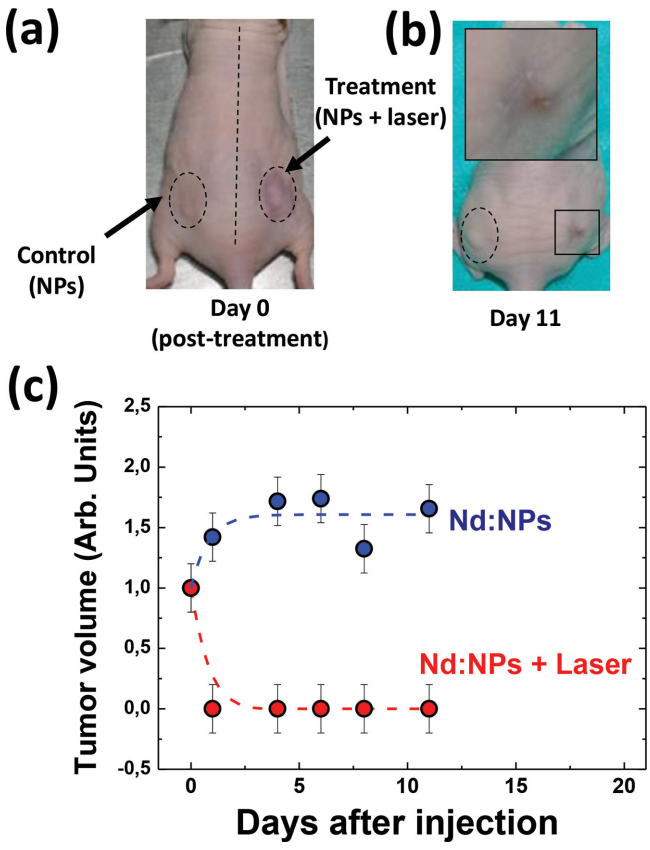

Figure 8. a) Optical image of a representative mouse with two tumors, both injected with a solution containing Nd:LaF_3 NPs. The left-side tumor was used as a control (without laser irradiation) whereas the right-side tumor was subjected to photothermal treatment (PTT) by irradiating it with a 808 nm laser beam (4 W/cm^2). The picture was taken just after the PTT. b) Optical image of the same mouse taken 11 days after treatment. The size evolution of both treated and control tumors is included in (c). Symbols are experimental data and dashed lines are guides for the eyes.

the observed preferential retention of Nd:LaF_3 NPs by liver and spleen is also in agreement with the analysis of in vivo images of healthy mice after intravenous injections and that were previously explained in terms of their negatively charged coating. In this respect, the Z-potential of the 5.6 at% doped LaF_3 NPs has been experimentally found to be –23.7 mV (see the Z-potential spectrum included in the Supporting Information, Figure S4).[34] Therefore, we claim that a small portion of the NPs initially injected in the tumor reaches the bloodstream and is finally accumulated in the spleen.

In order to unequivocally relate the successful tumor eradication to the tumor heating induced in vivo by the irradiation of Nd:LaF_3 NPs, we used a different group of animals. In this case, both tumors were injected with a solution containing Nd:LaF_3 NPs but only one of them was treated with the 808 nm laser (see **Figure 8**a). Irradiation conditions were the same as those employed in Figure 5, and dynamical intratumoral thermal measurements revealed practically identical heating curves as those included in Figure 5d. Figure 8b shows an optical image of the mouse after the treatment, revealing the complete elimination of the tumor subjected to PTT with the only sequel of an uninfected scar. The time evolution of both treated and control tumor volumes is shown in Figure 8c and clearly reveals that efficient treatment was only achieved in the laser irradiated tumor.

We also conducted a series of in vitro experiments that were aimed to determine whether or not Nd:LaF_3 NPs are toxic by themselves to the MB-MDA-231 breast cancer cells. For this purpose we used the MTT assay for cell viability 24 h after exposing the cell cultures to NPs dispersed in the culture medium. We tested two different concentrations and 5 different incubation times. In agreement with our in vivo results, the Nd:LaF_3 NPs did not cause relevant toxicity to MDA-MB-231 cells under any of the different experimental conditions (see Figure S5 in the Supporting Information). Both in vivo and in vitro results indicated that the presence of Nd:LaF_3 NPs on their own is not toxic for cancer cells and, consequently, has no therapeutic effect on the tumor. This conclusion strongly supports the potential use of Nd:LaF_3 NPs for effective and highly controlled combined photothermal and bioimaging therapeutic techniques that could provide renewed expectations in the field of cancer treatment.

3. Conclusions

In summary, the experiments performed in this work clearly demonstrate that it is possible to perform in vivo efficient temperature-controlled photothermal therapy of cancer tumors by using highly Nd^{3+} ion doped LaF_3 biocompatible nanoparticles. These nanoparticles act, at the same time, as infrared light excited nanoheaters and fluorescent thermal nanosensors, based on the particular excitation and de-excitation features of the Neodymium ions. We demonstrate that non-invasive intratumoral temperature reading during hyperthermia treatment is possible from a simple analysis of the intratumoral fluorescence generated by the Nd^{3+} ion doped LaF_3 nanoparticles. Intratumoral temperature measurements have highlighted the importance of using the actual intratumoral temperature for therapy adjustment and control instead of the traditionally used surface (skin) temperature. The results obtained in this work open a new avenue towards the clinical application of nanoparticle-based photothermal therapy.

4. Experimental Section

Synthesis of Nd:LaF_3 Nanoparticles: The Nd^{3+} doped LaF_3 NPs used in this work were prepared by wet-chemistry method. Lanthanum (III) chloride ($LaCl_3$, 99.9%), Neodymium (III) chloride ($NdCl_3$, 99.9%), and ammonium fluoride (NH_4F, 99.9%), were purchased from Sigma-Aldrich. All reagents were used directly, without further purification. Typically, $(1 - x)$ mmol of $LaCl_3$, x mmol of $NdCl_3$ (x = 5, 10,15, 20, and 25 in%) were added to 80 mL DI water in a round bottom single neck flask under continuous stirring for 15 min, and heated to 75 °C. Then 3 mmol of NH_4F was diluted in 3 ml DI water and added dropwise to the above mixed chemical solution. The mixture was kept at 75 °C for 3 h at ambient pressure under continuous stirring. A white suspension was formed gradually upon stirring. The obtained NPs were collected by centrifugation at 8000 rpm for 7 min. The precipitate was washed with distilled water several times and finally centrifuged at 12 000 rpm for 12 min and dried at 60 °C at ambient atmosphere for 18 h.

Structural and Elemental Analysis: The X-ray diffraction (XRD) patterns were collected on a Shimadzu X-ray diffractometer (XRD-6000) with

Cu-Kα radiation (λ = 1.5405 Å, Power of 30 kV × 20 mA) to identify the possible phases in 10–90° (2θ) range with a scanning rate of 0.60 °C/min and 0.02° step size. Figure S6 shows the XRD spectrum of 5.6 at% doped Nd:LaF_3 nanoparticles denoting the existence of a pure hexagonal phase of LaF_3. The powder samples were thoroughly grinded in a mortar and then deposited in a low-background sample stage for the collection. The particle size and morphology were evaluated using transmission electron microscope (TEM, TECNAI G2 with resolution 0.2 nm) with an accelerating voltage of 200 kV. For TEM investigations, powders were suspended in methanol-water mixture, and a drop of this suspension was deposited on a holey carbon-coated film supported on a 300 mesh copper grid. Inset in Figure S7 shows the TEM image of the Nd:LaF_3 nanoparticles used for in vivo photothermal treatments. The size histogram resulting from the analysis of this TEM image is also included indicating an average diameter of 12 nm. Energy dispersive X-ray (EDX) spectroscopy was done using a Hitachi TM-3000 (table top) scanning electron microscope, operated at 15 kV. Dry powdered samples were attached to the substrate using a double-sided carbon tape, and mounted onto the sample holder. The Fourier transform infrared spectra (FTIR) of the samples were recorded in the range of 400–4000 cm^{-1} on a Shimadzu IRPrestige-21 FTIR spectrophotometer using the KBr pellet method. Figure S8 includes the FTIR spectrum of 5.6 at% Neodymium doped Nd:LaF_3 nanoparticles.

Absorption and Fluorescence Measurements: The absorption spectra were measured on a UV/VIS/NIR spectrophotometer (PerkinElmer LAMBDA 1050) with a resolution of 0.5 nm. Fluorescence characterization of the synthesized nanocrystals was performed by using either a 808 nm fiber coupled laser diode or a continuous wave tunable Ti:Sapphire laser. Fluorescence was collected by a set of lenses and spectrally analyzed by a high resolution spectrometer (Horiba iHR500) and a Peltier cooler CCD detector (Synapse Horiba). Thermal images were obtained by using a FLIR E40 thermal camera.

In Vitro Cell via Bility/Cytotoxicity Studies: The MTT (3-(4,5-dimethylthiazol-2-yl)-2,5-diphenyltetrazolium bromide) assay is a simple non-radioactive colorimetric assay to measure cell cytotoxicity, proliferation or viability. MTT is a yellow, watersoluble, tetrazolium salt. Metabolically active cells are able to convert this dye into a water-insoluble dark blue formazan by reductive cleavage of the tetrazolium ring.[35] Formazan crystals, then, can be dissolved in an organic solvent such as dimethylsulphoxide (DMSO) and quantified by measuring the absorbance of the solution at 540 nm, and the resultant value is related to the number of living cells. To determine cell cytotoxicity/viability, the cells were plated in a 24 well plate at 37 °C in 5% CO_2 atmosphere. After 48 h of culture, the medium in the well was replaced with the fresh medium containing nanoparticles of two different concentrations (400 µg/mL and 200 µg/mL) and cells were incubated for different periods of time (2, 5, 8, 15, and 24 h). After incubation, the medium was removed and added completed medium without nanoparticles. After 24 h, 0.5 mL of MTT dye solution (0.05 mg/mL of MTT, Sigma) was added to each well. After 2–3 h of incubation at 37 °C and 5% CO_2, the medium was removed and formazan crystals were solubilized in 0.5 mL of DMSO (Merck) and the solution was vigorously mixed to dissolve the reacted dye. The absorbance at 540 nm was read using a microplate reader (Espectra Fluor 4, Tecan). The% of viability of cells incubated with NPs as compared to control cells (i.e., without incubation with nanoparticles) was calculated as [A] test/[A] control ×100, where [A] test is the absorbance of the tested sample and [A] control is the absorbance of the control sample.

Animal Experiments: For the analysis of the biodistribution pattern of Nd:LaF_3 NPs we used CD1 mice. For the tumor xenograft model, we used 6 female athymic nude mice (Harlan) aged 9–16 weeks and with a weight of 28–32 g at the beginning of the experiments. The animals were subcutaneously inoculated in both flanks with 10×10^6 MDA-MB-231 cells per flank resuspended in a volume of 200 µl of PBS. Tumor size or ulceration was evaluated daily during 20 days starting the day after the treatment. When the tumors reached a minimum volume of 9 mm^3, we proceeded to apply the treatment with thermal control, using in each animal one tumor as an internal control with only NPs or laser irradiation and the other one with the complete treatment (NPs + laser irradiation). For the treatment, the mice were anesthetized with 2% isoflurane and a PBS based solution containing 25 at% Neodymium doped LaF_3 nanoparticles was inoculated in the tumor. The concentration of LaF_3 nanoparticles in the solution was 50 µg/mL. The inoculated volume of nanoparticles solution was calculated as ½ of the total tumor volume. The control tumors with only laser irradiation were inoculated with the same volume of PBS. Laser excitation was achieved by using a fiber coupled 808 nm laser diode. The 808 nm laser intensity was monitored all along the experiments by controlling both the laser power and the laser spot size. For tumor treatment the spot size was set to three times the tumor section and the laser power was adjusted to achieve a laser intensity of 4 W/cm^2. For whole animal imaging the spot size was set to 6 cm^2 and laser power was adjusted to achieve a laser intensity of 1 W/cm^2. Infrared fluorescence images were acquired by using a XEva 17 AsGaIn CCD camera with enhanced sensitivity in the 1000–1700 nm spectral range. A long pass filter with cut-off wavelength at 850 nm was used to remove the 808 nm pump background. For intratumoral temperature determination, the fluorescence generated by the injected Nd:LaF_3 nanoparticles was collected by placing a low numerical aperture optical fiber 1 cm from the tumor surface. The fiber was connected to a high-resolution spectrometer so that it was spectrally analysed in the 850–1000 nm range with a spatial resolution better than 0.2 nm. Acquisition time was 1 s and real time determination of temperature was achieved by using a simple algorithm to the measured spectra that allowed real time determination of the spectral ratio between the different fluorescence bands. The surface temperature was simultaneously measured by using an infrared thermal camera (Fluke Ti10). Mice were housed and maintained under specific pathogen-free conditions and provided with food and water ad libitum. All the experimental procedures with animals were carried out in compliance with the guidelines in RD 53/2013 (Spain) and were approved by the Ethics Committee from Universidad Autonóma de Madrid (CEIT) in the frame of the project FIS-PI12/01253 supported by the Spanish Ministerio de Economía y Competitividad.

Supporting Information

Supporting Information is available from the Wiley Online Library.

Acknowledgements

The work was supported by the Ministerio de Innovación y Ciencia of Spain under projects MAT2010–16161 and MAT2013–47395-C4–1-R. P.H. thanks the Spanish Ministerio de Economia y Competitividad (MINECO) for a Juan de la Cierva grant. The authors also thank the Brazilian agencies FAPEAL-Fundação de Amparo a Pesquisa do Estado de Alagoas (Project PRONEX 2009–09–006), FINEP (Financiadora de Estudos e Projetos), CNPq (Conselho Nacional de Desenvolvimento Científico e Tecnológico) through Grant INCT NANO(BIO)SIMES, and CAPES (Coordenadoria de Aperfeiçoamento de Pessoal de Ensino Superior). D.J. (Pesquisador Visitante Especial(PVE)-CAPES) thanks the CAPES by means of the Project PVE number A077/2013. B. del Rosal thanks Universidad Autónoma de Madrid for an FPI grant.

Received: October 19, 2014
Published online: December 6, 2014

[1] a) M. Ferrari, *Nat. Rev. Cancer* **2005**, *5*, 161; b) S. M. Nie, Y. Xing, G. J. Kim, J. W. Simons, *Ann. Rev. Biomed. Eng.* **2007**, *9*, 257.
[2] L. Y. Ang, M. E. Lim, L. C. Ong, Y. Zhang, *Nanomedicine* **2011**, *6*, 1273.

[3] a) R. Abdul Jalil, Y. Zhang, *Biomaterials* **2008**, *29*, 4122; b) Y. He, Y. Zhong, Y. Su, Y. Lu, Z. Jiang, F. Peng, T. Xu, S. Su, Q. Huang, C. Fan, *Angew. Chem. Int. Ed.* **2011**, *50*, 5695; c) A. M. Smith, S. Dave, S. Nie, L. True, X. Gao, *Exp. Rev. Mol. Diagnostics* **2006**, *6*, 231; d) H. Wang, T. B. Huff, D. A. Zweifel, W. He, P. S. Low, A. Wei, J.-X. Cheng, *Proc. Natl. Acad. Sci. U.S.A.* **2005**, *102*, 15752; e) D. K. Chatterjee, M. K. Gnanasammandhan, Y. Zhang, *Small* **2010**, *6*, 2781; f) A. Gnach, A. Bednarkiewicz, *Nano Today* **2012**, *7*, 532; g) S. A. Hilderbrand, F. W. Shao, C. Salthouse, U. Mahmood, R. Weissleder, *Chem. Commun.* **2009**, 4188; h) F. Vetrone, R. Naccache, A. J. d. l. Fuente, F. Sanz-Rodríguez, A. Blazquez-Castro, E. M. Rodriguez, D. Jaque, J. G. Solé, J. A. Capobianco, *Nanoscale* **2010**, *2*, 495; i) F. Wang, D. Banerjee, Y. S. Liu, X. Y. Chen, X. G. Liu, *Analyst* **2010**, *135*, 1839.

[4] I. L. Medintz, H. T. Uyeda, E. R. Goldman, H. Mattoussi, *Nat. Mater.* **2005**, *4*, 435.

[5] a) F. Alexis, E. Pridgen, L. K. Molnar, O. C. Farokhzad, *Mol. Pharmaceutics* **2008**, *5*, 505; b) N. Khlebtsov, L. Dykman, *Chem. Soc. Rev.* **2011**, *40*, 1647; c) Z. Liu, C. Davis, W. B. Cai, L. He, X. Y. Chen, H. J. Dai, *Proc. Natl. Acad. Sci. U.S.A.* **2008**, *105*, 1410; d) J. T. Robinson, K. Welsher, S. M. Tabakman, S. P. Sherlock, H. L. Wang, R. Luong, H. J. Dai, *Nano Res.* **2010**, *3*, 779.

[6] K. T. Yong, J. Qian, I. Roy, H. H. Lee, E. J. Bergey, K. M. Tramposch, S. He, M. T. Swihart, A. Maitra, P. N. Prasad, *Nano Lett.* **2007**, *7*, 761.

[7] D. K. Chatterjee, L. S. Fong, Y. Zhang, *Adv. Drug Delivery Rev.* **2008**, *60*, 1627.

[8] S. Sortino, *J. Mater. Chem.* **2012**, *22*, 301.

[9] a) M. L. Mastronardi, F. Maier-Flaig, D. Faulkner, E. J. Henderson, C. Kübel, U. Lemmer, G. A. Ozin, *Nano Lett.* **2011**, *12*, 337; b) L. M. Maestro, C. Jacinto, U. Rocha, M. C. I.-d. l. Cruz, F. Sanz-Rodriguez, A. Juarranz, J. G. Solé, D. Jaque, *J. Apll. Phys.* **2012**, *111*, 023513.

[10] B. H. a. G. F. Imbusch, *Optical Spectroscopy of Inorganic Solids* Oxford Science, New York **1989**.

[11] I. H. El-Sayed, X. Huang, M. A. El-Sayed, *Cancer Lett.* **2006**, *239*, 129.

[12] H. K. Moon, S. H. Lee, H. C. Choi, *ACS Nano* **2009**, *3*, 3707.

[13] a) A. Chicheł, J. Skowronek, M. Kubaszewska, M. Kanikowski, *Rep. Practical Oncol. Radiother.* **2007**, *12*, 267; b) L. E. Gerweck, *Cancer Res.* **1985**, *45*, 3408; c) R. W. Habash, R. Bansal, D. Krewski, H. T. Alhafid, *Crit. Rev. Biomed. Eng.* **2006**, *34*, 459; d) R. W. Habash, R. Bansal, D. Krewski, H. T. Alhafid, *Crit. Rev. Biomed. Eng.* **2006**, *34*, 491; e) R. W. Habash, R. Bansal, D. Krewski, H. T. Alhafid, *Crit. Rev. Biomed. Eng.* **2007**, *35*, 37; f) J. G. Short, P. F. Turner, *Proc. IEEE* **1980**, *68*, 133; g) N. A. Armar, G. C. L. Lachelin, *Int. J. Obstetrics Gynaecol.* **1993**, *100*, 161; h) J. R. Lepock, K.-H. Cheng, H. Al-qysi, I. Sim, C. J. Koch, J. Kruuv, *Int. J. Hyperthermia* **1987**, *3*, 123; i) K. J. Henle, L. A. Dethlefsen, *Cancer Res.* **1978**, *38*, 1843; j) A. E. Caccamo, S. Desenzani, L. Belloni, A. F. Borghetti, S. Bettuzzi, *J. Cell. Physiol.* **2006**, *207*, 208; k) P. Chakravarty, R. Marches, N. S. Zimmerman, A. D.-E. Swafford, P. Bajaj, I. H. Musselman, P. Pantano, R. K. Draper, E. S. Vitetta, *Proc. Natl. Acad. Sci.* **2008**, *105*, 8697; l) J. L. Roti Roti, *Int. J. Hyperthermia* **2008**, *24*, 3.

[14] J. R. Whitney, S. Sarkar, J. Zhang, T. Do, T. Young, M. K. Manson, T. A. Campbell, A. A. Puretzky, C. M. Rouleau, K. L. More, D. B. Geohegan, C. G. Rylander, H. C. Dorn, M. N. Rylander, *Lasers Surg. Med.* **2011**, *43*, 43.

[15] E. B. Dickerson, E. C. Dreaden, X. H. Huang, I. H. El-Sayed, H. H. Chu, S. Pushpanketh, J. F. McDonald, M. A. El-Sayed, *Cancer Lett.* **2008**, *269*, 57.

[16] J. Chen, C. Glaus, R. Laforest, Q. Zhang, M. Yang, *Small* **2010**, *6*, 811.

[17] J. Robinson, K. Welsher, S. Tabakman, S. Sherlock, H. Wang, R. Luong, H. Dai, *Nano Res.* **2010**, *3*, 779.

[18] Z.-S. Deng, J. Liu, *Comput. Biol. Med. 34*, 495.

[19] J. J. Crochet, S. C. Gnyawali, Y. Chen, E. C. Lemley, L. V. Wang, W. R. Chen, *J. Biomed. Opt.* **2006**, *11*, 034031.

[20] K. Van Alstyne, T. Olson, *Mar. Biol.* **2014**, *161*, 1409.

[21] C. D. Brites, P. P. Lima, N. J. Silva, A. Millan, V. S. Amaral, F. Palacio, L. D. Carlos, *Nanoscale* **2012**, *4*, 4799.

[22] D. Jaque, F. Vetrone, *Nanoscale* **2012**, *4*, 4301.

[23] J. S. Donner, S. A. Thompson, C. Alonso-Ortega, J. Morales, L. G. Rico, S. I. C. O. Santos, R. Quidant, *ACS Nano* **2013**, *7*, 8666.

[24] J. S. Donner, S. A. Thompson, M. P. Kreuzer, G. Baffou, R. Quidant, *Nano Lett.* **2012**, *12*, 2107.

[25] a) L. M. Maestro, P. Haro-González, M. C. Iglesias-de la Cruz, F. Sanz-Rodríguez, A. Juarranz, J. G. Solé, D. Jaque, *Nanomedicine* **2012**; b) G. Kucsko, P. C. Maurer, N. Y. Yao, M. Kubo, H. J. Noh, *Nature* **2013**, *500*, 54.

[26] a) R. R. Anderson, J. A. Parrish, *J. Investig. Dermatol.* **1981**, *77*, 13; b) A. M. Smith, M. C. Mancini, S. Nie, *Nat. Nanotechnol.* **2009**, *4*, 710.

[27] a) D. J. Naczynski, M. C. Tan, M. Zevon, B. Wall, J. Kohl, A. Kulesa, S. Chen, C. M. Roth, R. E. Riman, P. V. Moghe, *Nat. Commun.* **2013**, 4; b) Y. Zhang, G. Hong, Y. Zhang, G. Chen, F. Li, H. Dai, Q. Wang, *ACS Nano* **2012**, *6*, 3695; c) G. H. T. Au, W. Y. Shih, S.-J. Tseng, W.-H. Shih, *Nanotechology* **2012**, *23*, 275601; d) W. Jiang, A. Singhal, B. Y. S. Kim, J. Zheng, J. T. Rutka, C. Wang, W. C. W. Chan, *J. Assoc. Lab. Automation* **2008**, *13*, 6.

[28] a) A. E. Albers, E. M. Chan, P. M. McBride, C. M. Ajo-Franklin, B. E. Cohen, B. A. Helms, *J. Am. Chem. Soc.* **2012**, *134*, 9565; b) M. L. Debasu, D. Ananias, I. Pastoriza-Santos, L. M. Liz-Marzán, J. Rocha, L. D. Carlos, *Adv. Mater.* **2013**, *23*, 4868.

[29] U. Rocha, K. Upendra Kumar, C. Jacinto, J. Ramiro, A. J. Caamaño, J. García Solé, D. Jaque, *Appl. Phys. Lett.* **2014**, 053703.*104*

[30] U. Rocha, C. Jacinto da Silva, W. Ferreira Silva, I. Guedes, A. Benayas, L. Martínez Maestro, M. Acosta Elias, E. Bovero, F. C. J. M. van Veggel, J. A. García Solé, D. Jaque, *ACS Nano* **2013**, *7*, 1188.

[31] V. K. Rai, *Appl. Phys. B* **2007**, *88*, 297.

[32] F. Xu, K. A. Seffen, T. J. Lu, *Int. J. Heat Mass Transfer* **2008**, *51*, 2237.

[33] I. Villa, A. Vedda, I. Cantarelli, M. Pedroni, F. Piccinelli, M. Bettinelli, A. Speghini, M. Quintanilla, F. Vetrone, U. Rocha, C. Jacinto, E. Carrasco, F. Rodríguez, Á. Juarranz, B. del Rosal, D. Ortgies, P. Gonzalez, J. Solé, D. García, *Nano Res.* **2014**, 1.

[34] U. Rocha, K. U. Kumar, C. Jacinto, I. Villa, F. Sanz-Rodríguez, M. del Carmen Iglesias de la Cruz, A. Juarranz, E. Carrasco, F. C. J. M. van Veggel, E. Bovero, J. G. Solé, D. Jaque, *Small* **2013**.

[35] T. Mosmann, *J. Immunol. Methods* **1983**, *65*, 55.

[36] S. Zheng, W. Chen, D. Tan, J. Zhou, Q. Guo, W. Jiang, C. Xu, X. Liu, J. Qiu, *Nanoscale* **2014**, *6*, 5675.

[37] V. Lojpur, M. Nikolic, L. Mancic, O. Milosevic, M. Dramicanin, *Ceramics Int.* **2013**, *39*, 1129.

[38] A. Pandey, V. K. Rai, *Dalton Trans.* **2013**, *42*, 11005.

[39] W. Xu, H. Zhao, Y. Li, L. Zheng, Z. Zhang, W. Cao, *Sens. Actuators B: Chem.* **2013**, *188*, 1096.

[40] N. Dong, M. Pedroni, F. Piccinelli, G. Conti, A. Sbarbati, J. R. Hernandez, L. M. Maestro, M. C. Iglesias de la Cruz, F. Sanz-Rodriguez, A. Juarranz, *ACS Nano* **2011**.

[41] D. Wawrzynczyk, A. Bednarkiewicz, M. Nyk, W. Strek, M. Samoc, *Nanoscale* **2012**, *4*, 6959.

[42] B. N. Khlebtsov, E. V. Panfilova, G. S. Terentyuk, I. L. Maksimova, A. V. Ivanov, N. G. Khlebtsov, *Langmuir* **2012**, *28*, 8994.

[43] G. S. Terentyuk, A. V. Ivanov, N. I. Polyanskaya, I. L. Maksimova, A. A. Skaptsov, D. S. Chumakov, B. N. Khlebtsov, N. G. Khlebtsov, *Quantum Electron.* **2012**, *42*, 380.

[44] F. Zhou, D. Xing, Z. Ou, B. Wu, D. E. Resasco, W. R. Chen, *J. Biomed. Opt.* **2009**, *14*, 021009.
[45] A. Burke, X. Ding, R. Singh, R. A. Kraft, N. Levi-Polyachenko, M. N. Rylander, C. Szot, C. Buchanan, J. Whitney, J. Fisher, H. C. Hatcher, R. D'Agostino, N. D. Kock, P. M. Ajayan, D. L. Carroll, S. Akman, F. M. Torti, S. V. Torti, *Proc. Natl. Acad. Sci.* **2009**, *106*, 12897.
[46] N. Huang, H. Wang, J. Zhao, H. Lui, M. Korbelik, H. Zeng, *Lasers Surg. Med.* **2010**, *42*, 798.
[47] K. Yang, S. Zhang, G. Zhang, X. Sun, S. T. Lee, Z. Liu, *Nano Lett.* **2010**, *10*, 3318.
[48] K. Yang, J. Wan, S. Zhang, B. Tian, Y. Zhang, Z. Liu, *Biomaterials* **2012**, *33*, 2206.
[49] K. Yang, H. Xu, L. Cheng, C. Sun, J. Wang, Z. Liu, *Adv. Mater.* **2012**, *24*, 5586.
[50] L. Cheng, W. He, H. Gong, C. Wang, Q. Chen, Z. Cheng, Z. Liu, *Adv. Funct. Mater.* **2013**, *23*, 5893.